



HAL
open science

Coupled modelling of redox reactions and glass melt fining processes

Franck Pigeonneau

► **To cite this version:**

Franck Pigeonneau. Coupled modelling of redox reactions and glass melt fining processes. Glass Technology - European Journal of Glass Science and Technology Part A, 2007. hal-01442935

HAL Id: hal-01442935

<https://hal.science/hal-01442935>

Submitted on 6 May 2017

HAL is a multi-disciplinary open access archive for the deposit and dissemination of scientific research documents, whether they are published or not. The documents may come from teaching and research institutions in France or abroad, or from public or private research centers.

L'archive ouverte pluridisciplinaire **HAL**, est destinée au dépôt et à la diffusion de documents scientifiques de niveau recherche, publiés ou non, émanant des établissements d'enseignement et de recherche français ou étrangers, des laboratoires publics ou privés.

Coupled modelling of redox reactions and glass melt fining processes

Franck Pigeonneau
Saint-Gobain Recherche
39 quai Lucien Lefranc - BP 135
93303 Aubervilliers cedex, France

February 21, 2015

Abstract

The quality of glass depends upon the removal of dissolved gases and bubbles. A quantitative understanding of these processes is essential for glass production today, where quality requirements are becoming increasingly stringent. Classical fining involves adding an element or compound to the melt which will, through oxidation-reduction reactions at high temperatures, produce gases that diffuse into the bubbles present in the melt. The growth of these bubbles then enhances the rate of bubble removal from the melt. The modelling of oxidation-reduction reactions and that of fining are generally treated independently from one another. However, due to the large number of bubbles present, a significant amount of dissolved gases are consumed and chemical equilibrium in the melt is changed. We present, in this paper, a theoretical model where redox equilibrium is coupled with bubble generator and growth. Our approach is similar to that proposed by Nemeč and his co-workers [7, 14], but differs in the numerical method. After a description of the model, we present the evolution of a bubble population with time and also apply the numerical method to an experimental tool where bubbling is used to equilibrate the partial pressures between the bubbles and between the melt. We find, with the model, an equilibrium time longer than seen experimentally. The possible origins of the disagreement are investigated and discussed.

Introduction

Molten soda-lime-silica glass is obtained from, among other things, carbonaceous raw materials such as $CaCO_3$ and Na_2CO_3 . These release CO_2 gas which is then found in the molten glass partly in bubble form and partly dissolved in the melt. Nemeč and Klouzek [10] indicate that the bubble concentration can approach 10^9 bubbles per cubic meter. Since the final product must have the fewest bubbles possible, the goal of the fining process is to eliminate a large number of the bubbles present in the glass.

Bubble evacuation is a difficult task in a viscous fluid such as molten glass due to the low rise velocity especially for small bubbles with diameters less than 0.5 mm. This velocity increases with temperature due to decreasing viscosity and with increasing bubble size. Moreover, though the addition of “fining” agents, the bubble size can be increased due to the migration of “fining” gases dissolved in the molten glass towards the bubbles. Finding good fining agents is the art of a glass maker. Optimization of these agents can be achieved through the use of experimental devices and by modelling the fining process.

As previously mentioned, most fining processes are governed by the oxidation-reduction reactions of fining agents. In many investigations [1] these two phenomena are treated separately with, in the first stage, redox behavior in the glass being determined and, secondly, the evolution of the bubbles being studied. But due to the large number of bubbles, the consumption of dissolved gases can significantly change the redox state. Only a few publications by Nemeč and his

co-workers [7, 14] try to take into account the coupling of redox and fining. This article carries out the coupled modelling of these two processes in a system assumed to be spatially homogeneous.

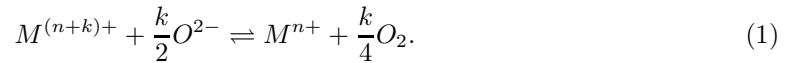
After the presentation of the basic equations of the model in section 1, the results are given in section 2 followed by a discussion and conclusion.

1 Modelling of redox and fining processes

In a glass melt at high temperatures, chemical reactions play an important role in the fining process [5]. Many gas species, such as water, oxygen, carbon dioxide and sulphur, react with glass and as indicated in the introduction, the fining of gas bubbles is supported by the addition of fining agents which react as the temperature increases. The chemical agents classically used are: sulphate, arsenic(V) oxide, antimony(V) oxide.

1.1 Redox model

Knowledge of the concentrations of dissolved gases is necessary in order to describe the evolution of bubbles. These concentrations depend on reduction-oxidation reactions. We assume that locally these reactions are in a state of chemical equilibrium, an assumption that has been justified by Russel [12]. Consider a polyvalent chemical element, M . The reduction reaction of the polyvalent ion M is given by [13]



M^{n+} and $M^{(n+k)+}$ represent, respectively the reduced and oxidized states of M . The equilibrium constant of this reaction is given by the following equation [2]

$$K_M = \frac{C_{M^{n+}} C_{O_2}^{k/4}}{C_{M^{(n+k)+}}}. \quad (2)$$

$C_{M^{n+}}$, C_{O_2} and $C_{M^{(n+k)+}}$ are molar concentrations.

The modelling of reduction-oxidation reactions is presented here under a general form where we assume that R reactions take place in the glass melt. The number of ionic species is N_I and the number of fining gas species is N_{fg} . The generic reaction r is thus written

$$\sum_{i=1}^{N_I} \nu'_{ri} \mathfrak{A}_i + \sum_{j=1}^{N_{fg}} \beta'_{rj} \mathfrak{G}_j \rightleftharpoons \sum_{i=1}^{N_I} \nu''_{ri} \mathfrak{A}_i + \sum_{j=1}^{N_{fg}} \beta''_{rj} \mathfrak{G}_j. \quad (3)$$

\mathfrak{A}_i is the ion i where i varies from 1 to N_I and \mathfrak{G}_j corresponds to the gas j where j varies from 1 to N_{fg} . The stoichiometric coefficients for ionic and gas species taken into account in reaction r are defined by the following relations [11]

$$\nu_{ri} = \nu''_{ri} - \nu'_{ri}, \text{ for } i = 1 \text{ to } N_I. \quad (4a)$$

$$\beta_{rj} = \beta''_{rj} - \beta'_{rj}, \text{ for } j = 1 \text{ to } N_{fg}. \quad (4b)$$

The equilibrium constant of reaction r is given by [11]

$$K_r = \prod_{i=1}^{N_I} C_{\mathfrak{A}_i}^{\nu_{ri}} \prod_{j=1}^{N_{fg}} C_{\mathfrak{G}_j}^{\beta_{rj}} = \exp\left(\frac{-\Delta G_r}{\mathcal{R}T}\right), \quad (5)$$

where ΔG_r is the Gibbs free energy of reaction r defined by

$$\Delta G_r = \Delta H_r - T\Delta S_r. \quad (6)$$

ΔH_r and ΔS_r are, respectively, the enthalpy and entropy of reaction r , \mathcal{R} is the universal gas constant and T the temperature.

The determination of ionic and gaseous concentrations is carried out by setting the chemical affinity equal to zero for each of the R reactions due to the assumption of chemical equilibrium. Before presenting how this is achieved, the fining model will be described.

1.2 Fining model

Gas bubbles contained in the glass melt must be removed. As noted by Beerkens [1], primary fining is the removal of bubbles through the action of fining agents releasing gases in order to enhance bubble growth. Since the rise velocity of a bubble is proportional to its radius squared, the time required for a bubble to reach the glass melt surface decreases with bubble growth. Primary fining is relevant at high temperature while secondary fining is the re-absorption of bubbles during cooling of the melt. As temperature decreases, the chemical solubility of species like O_2 , SO_2 increases. This effect leads to a reduction in bubble size.

Both bubble growth and shrinkage are controlled by mass transfer between bubble and melt. This process also takes into account multispecies diffusion. A detailed model can be found in reference [1]. Here, we begin by outlining the mass transfer laws of gases diffusing into bubbles moving in a melt. Afterwards, the equations describing the dynamic variation of bubble position, radius and partial pressures will be specified.

1.2.1 Mass transfer

Assuming that bubbles are composed of N_g gases (where $N_g = N_{fg} + N_{nfg}$ and N_{nfg} corresponds to the number of non-fining gases such N_2 or H_2O), the number of moles of gas species \mathfrak{G}_j can be determined by

$$\frac{dn_{\mathfrak{G}_j}}{dt} = 4\pi a^2 k_{\mathfrak{G}_j} (C_{\mathfrak{G}_j} - C_{\mathfrak{G}_j}^s), \quad (7)$$

where $n_{\mathfrak{G}_j}$ is the number of moles of gas species \mathfrak{G}_j , a the bubble radius, $k_{\mathfrak{G}_j}$ the mass transfer coefficient, $C_{\mathfrak{G}_j}$ the bulk molar concentration, $C_{\mathfrak{G}_j}^s$ the molar concentration at the bubble surface.

The mass transfer coefficient is derived from the Sherwood number.

$$Sh_{\mathfrak{G}_j} = \frac{2ak_{\mathfrak{G}_j}}{D_{\mathfrak{G}_j}}. \quad (8)$$

$D_{\mathfrak{G}_j}$ is the diffusion coefficient of species \mathfrak{G}_j . Mass transfer is also influenced by the velocity of the bubble relative to the molten glass. The importance of this motion is quantified by the Péclet number

$$Pe_{\mathfrak{G}_j} = \frac{2au_b}{D_{\mathfrak{G}_j}}. \quad (9)$$

u_b is the bubble velocity relative to the molten glass. If we assume that the bubble interface is rigid, the Sherwood number must be proportional to the Peclet number to the power of one-third. Here we use the law given in the textbook of Clift *et al* [4]:

$$Sh_{\mathfrak{G}_j} = 1 + (1 + Pe_{\mathfrak{G}_j})^{1/3}. \quad (10)$$

This equation agrees with the numerical solution within 2% over a large range of Péclet numbers. This is established for Stokes flow in an infinite domain however equation (10) can only be used for $Re \leq 1$ (see for details [4]) where Re is the Reynolds number given by

$$Re = \frac{2au_b\rho}{\mu}. \quad (11)$$

ρ is glass density and μ dynamical viscosity.

The surface concentration, $C_{\mathfrak{G}_j}^s$, is determined using Henry's law:

$$C_{\mathfrak{G}_j}^s = L_{\mathfrak{G}_j} P_{\mathfrak{G}_j}^{\alpha_{\mathfrak{G}_j}}, \quad (12)$$

where $L_{\mathfrak{G}_j}$ is the solubility coefficient, $P_{\mathfrak{G}_j}$ is the partial pressure of the species \mathfrak{G}_j in the bubble and $\alpha_{\mathfrak{G}_j}$ is a stoichiometric coefficient equal to unity for most species but is equal to 1/2 for water [1].

1.2.2 Bubble growth and shrinkage

To describe the evolution of radius and partial pressure in a bubble, we use the ideal gas law:

$$PV = \mathcal{R}T \sum_{j=1}^{N_g} n_{\mathfrak{G}_j}, \quad (13)$$

where P is the total pressure in the bubble and V bubble volume. For each species \mathfrak{G}_j , we have

$$P_{\mathfrak{G}_j}V = n_{\mathfrak{G}_j}\mathcal{R}T. \quad (14)$$

The total pressure and partial pressures are linked by Dalton's law:

$$P = \sum_{j=1}^{N_g} P_{\mathfrak{G}_j}, \quad (15)$$

and the total pressure is defined by the following expression

$$P = P_0 + \rho g(h - z) + \frac{2\sigma}{a}, \quad (16)$$

where P_0 is the atmospheric pressure above the melt; h glass height; z the vertical position and σ the surface tension.

The equations describing the change of radius and partial pressure over time are obtained by the derivation, with respect to time, of the relations (13) and (14) and by inserting the expressions (7) and (16) (see [1]). The rise velocity, growth/skrinkage rate and change in partial pressure are given by

$$\frac{dz}{dt} = \frac{2\rho g a^2}{9\mu}, \quad (17a)$$

$$\begin{aligned} \frac{da}{dt} = & \frac{2\rho^2 g^2 a^3}{27\mu(P - 2\sigma/3a)} + \frac{\mathcal{R}T}{P - 2\sigma/3a} \sum_{j=1}^{N_g} k_{\mathfrak{G}_j} \left(C_{\mathfrak{G}_j} - L_{\mathfrak{G}_j} P_{\mathfrak{G}_j}^{\alpha_{\mathfrak{G}_j}} \right) + \\ & \frac{aP}{3(P - 2\sigma/3a)} \left(\frac{1}{T} \frac{dT}{dt} - \frac{1}{P} \frac{dP_0}{dt} \right), \end{aligned} \quad (17b)$$

$$\frac{dP_{\mathfrak{G}_j}}{dt} = \frac{3\mathcal{R}T}{a} k_{\mathfrak{G}_j} \left(C_{\mathfrak{G}_j} - L_{\mathfrak{G}_j} P_{\mathfrak{G}_j}^{\alpha_{\mathfrak{G}_j}} \right) + \frac{P_{\mathfrak{G}_j}}{T} \frac{dT}{dt} - \frac{3P_{\mathfrak{G}_j}}{a} \frac{da}{dt}, \text{ for } j = 1 \text{ to } N_g - 1. \quad (17c)$$

In these equations, we have taken into account the possibility of varying atmospheric pressure and temperature.

1.3 Coupled models

In the two preceding subsections, the reduction-oxidation and fining processes have been presented independently. Due to the large quantity of bubbles, the consumption of dissolved gases changes the redox state of glass. Here, we present a coupled model similar to that previously presented by Klouzek and Nemeč [7] and Matyas and Nemeč [9]. The domain is assumed to be spatially homogeneous which means that spatial derivatives of all quantities are equal to zero. In other words, only time is taken into account as a parameter.

In order to describe both the reduction-oxidation state and the fining process, we must first determine the behavior of ionic and gas species in molten glass with respect to time. The temporal

evolution of ionic and dissolved gases can be written as (see [7, 9, 11])

$$\frac{dC_{\mathfrak{A}_i}}{dt} = \sum_{r=1}^R \nu_{ri} \frac{d\zeta_r}{dt}, \text{ for } i = 1 \text{ to } N_I. \quad (18a)$$

$$\frac{dC_{\mathfrak{G}_j}}{dt} = \sum_{r=1}^R \beta_{rj} \frac{d\zeta_r}{dt} + S_{b,\mathfrak{G}_j}, \text{ for } j = 1 \text{ to } N_{fg} \text{ (fining gases)}, \quad (18b)$$

$$\frac{dC_{\mathfrak{G}_j}}{dt} = S_{b,\mathfrak{G}_j}, \text{ for } j = N_{fg} + 1 \text{ to } N_g \text{ (non-fining gases)}. \quad (18c)$$

$d\zeta_r/dt$ is the rate of reaction r - given in mol/(m³·s) - and S_{b,\mathfrak{G}_j} is the sink term due to the consumption of dissolved gas \mathfrak{G}_j . If the gas \mathfrak{G}_j goes from bubble to bulk, S_{b,\mathfrak{G}_j} becomes a source term.

S_{b,\mathfrak{G}_j} is determined using the evolution of the number of moles $n_{\mathfrak{G}_j}$ given by equation (7). If the number of bubbles with radius a is noted N_b , S_{b,\mathfrak{G}_j} is given by [7, 9]

$$S_{b,\mathfrak{G}_j} = -4\pi a^2 k_{\mathfrak{G}_j} \left(C_{\mathfrak{G}_j} - L_{\mathfrak{G}_j} P_{\mathfrak{G}_j}^{\alpha_{\mathfrak{G}_j}} \right) N_b. \quad (19)$$

To determine the evolution of $C_{\mathfrak{A}_i}$ and $C_{\mathfrak{G}_j}$, we must know the rate of reaction, $d\zeta_r/dt$. In order to find these values, we use the equilibrium constants for each reaction r defined by the equation (5). By taking the logarithmic derivate of (5), we have :

$$\sum_{i=1}^{N_I} \frac{\nu_{ri}}{C_{\mathfrak{A}_i}} \frac{dC_{\mathfrak{A}_i}}{dt} + \sum_{j=1}^{N_{fg}} \frac{\beta_{rj}}{C_{\mathfrak{G}_j}} \frac{dC_{\mathfrak{G}_j}}{dt} = \frac{d \ln K_r}{dT} \frac{dT}{dt}, \text{ for } r = 1 \text{ to } R. \quad (20)$$

Finally, using (18a) and (18b), we obtain a linear system of R equations:

$$\sum_{k=1}^R M_{rk} \frac{d\zeta_k}{dt} = \frac{d \ln K_r}{dT} \frac{dT}{dt} - \sum_{j=1}^{N_{fg}} \frac{\beta_{rj}}{C_{\mathfrak{G}_j}} S_{b,\mathfrak{G}_j}, \text{ for } r = 1 \text{ to } R. \quad (21)$$

The coefficients of the symmetric matrix \mathbb{M} , M_{rk} , are given by

$$M_{rk} = \sum_{i=1}^{N_I} \frac{\nu_{ri} \nu_{ki}}{C_{\mathfrak{A}_i}} + \sum_{j=1}^{N_{fg}} \frac{\beta_{rj} \beta_{kj}}{C_{\mathfrak{G}_j}}. \quad (22)$$

Thus, the rates of reaction are not equal to zero if the temperature varies or if there is a consumption of the dissolved gases is present.

At this stage, it is possible to numerically couple the redox behavior and fining process. The method is based on the numerical solution of the two systems (17) and (18) with (21) and the integration of the differential systems is carried out using the fourth order Runge-Kutta method.

2 Results

2.1 Fining evolution with coupled model

We consider a glass where the following two reduction-oxidation reactions take place



The enthalpy ΔH_r and entropy ΔS_r for these reactions are given in Table 3. These values come from reference [1]. The assumed concentrations of ionic and gaseous species at $T = 1200$ °C are given in Table 4.

The coupled model has been tested on bubble behavior in a soda-lime-silica glass melt. The height of the glass bath is taken to be 1 meter and the atmospheric pressure equal to 1 bar. The bubbles are composed of five gas species, two fining gases: O_2 and SO_2 and three non-fining gases: CO_2 , N_2 and H_2O . Initially, we assume that the bubble contains only CO_2 and that the radius is equal to $100 \mu\text{m}$ with the solubilities and diffusion coefficients for these elements taken from the data of Beerkens [1]. The concentrations of CO_2 , N_2 and H_2O in the glass are given in Table 5. We carried out two computations at $T = 1400$ °C: the first one with $N_b = 0$ and the second with $N_b = 10^8$ bubbles/ m^3 .

In Figure 1, we present the evolution of bubble radius as a function of the time for the two cases. The calculation is stopped when the bubble reaches the free surface. As can be seen, due to consumption of dissolved gases, the growth rate of the bubble decreases with an increasing concentration of bubbles. Indeed, the quantity of dissolved gas decreases with time, therefore, the gradient between the bulk and the bubble also decreases. We see also that the time needed by the bubble to reach the upper boundary is greater when $N_b = 10^8$ bubbles/ m^3 . For $N_b = 0$, this time is equal to 2.69 h and for $N_b = 10^8$ bubbles/ m^3 , it is equal to 3.21 h (*i.e.* a 20% of increase).

The influence of bubble concentration can also be observed on the evolution of molar fractions in the bubble presented in Figure 2 for the five gas species. Table 6 and Table 7 give the final molar fraction in each of the two cases. The molar fraction of O_2 in the bubble at the end of evolution is more important when $N_b = 10^8$ bubbles/ m^3 .

2.2 Equilibrium of gases in glass by bubbling

In this last subsection, we used the coupled method in order to find the time needed in order to equilibrate the glass with bubbles at certain initial concentrations. This is important if we wish to experimentally determine the equilibrium constants of reduction-oxidation reactions. The question is : how much time is necessary to reach a state of equilibrium? It is possible to use the coupled model presented in this article to realize this “numerical” experiment. We inject bubbles at a fixed gas flow rate into a crucible filled with one kilogram of glass. In order to reproduce bubbling flow, when a given bubble reaches the surface of the melt it is re-injected through the crucible bottom with its initial concentrations. The size and the concentration of bubbles are determined using bubbling laws previously detailed by Chavanne *et al* [3]. Computational tests have been performed at four temperatures: 1200, 1300, 1400 and 1500 °C. The radius and concentration of the bubbles are given in Table 8. The gas flow rate is fixed at 2 l/min under standard conditions ($T = 25$ °C and $P = 101325$ Pa) and we use the physical properties of a flat glass composition with the solubilities and diffusion coefficients being taken from Beerkens [1]. We assume air bubbles to mean that the molar fraction of O_2 is fixed at 0.21 and N_2 at 0.79. It should be specified that only the gases O_2 , SO_2 and N_2 are taken into account in this computation.

Figure 3 presents the evolution of O_2 activity in the glass as a function of time for the four temperatures. The evolution of P_{O_2} has three stages: in the first, the activity does not change; after that, we observe increasing P_{O_2} followed by a decrease and in the last stage, the P_{O_2} tends to the partial pressure fixed by the bubble. The equilibrium time reduces as the temperature increase. All these facts are physically intuitive, nevertheless, the equilibrium times found in this calculation are too large. Indeed, at $T = 1500$ °C, we find that the time to obtain equilibrium is approximatively equal to 16.7 days! A value which reaches 83 days at $T = 1400$ °C. In the “real” laboratory experiments, the order of magnitude is a few hours.

In order to improve these results, we have modified the Sherwood law. In fact, due to the large bubbles, the Reynolds number can be greater than one. With the sizes given in Table 8, Re is in the range of 9 to 120. We therefore use a different Sherwood law given by Clift *et al* [4] :

$$Sh = 0.991Pe^{1/3} \left(1 + \frac{Re}{4} \right)^{0.27} . \quad (24)$$

This equation is an extension of Levich’s law [8] for Reynolds numbers greater than one. However, even with this modification, the equilibrium times are not significantly changed. At 1600 °C, for example, equilibrium time is only reduced to 16 days, which is the same order of magnitude.

As presented by Beerkens and Waal [2] and by Beerkens [1], we have used an effective diffusion coefficient of O_2 in order to take into account the reaction of oxygen in the melt. This effective diffusion is evaluated using the same method proposed by Beerkens and Waal [2]. We find that the effective diffusivity is 6 times smaller than diffusion coefficient of O_2 on its own. However, the Sherwood number is proportional to the Péclet number to the power of one-third which means that decreasing the diffusivity by a factor 6 leads to only a factor 1.8 on the Sherwood number. Consequently, the disagreement between numerical results and experimental data presented here cannot explained by this effect. We need to take into account the effect of sulphate reaction and in that way couple the O_2 and SO_2 diffusivities.

Moreover, to describe bubble ascension, we have used Stokes’s law. However, the size of the bubble is not negligible compared to the crucible and therefore hydrodynamic interactions might impose a drag force on the bubbles (see reference [6]). Bubble velocity can thus, be decreased and this will affect also mass transfer. This improvement is outside of the scope of this article and will be addressed in the future.

The disagreement between model and experiment could also be due to the fact that, in the present method, the domain is spatially homogeneous and the mass transfer might be in fact controlled to local phenomena. This kind of description must take into account local advection and diffusion processes.

Conclusion

The objective of this investigation was the modelling of fining and redox processes. Due to the large quantity of bubbles present in glass during the first stage of melting, the consumption of dissolved gases can modify the redox state. In order to take this into consideration, we have presented a coupled model of redox reactions and fining processes. The method is based on the sequential solution of sets of differential equations, describing redox reaction and fining evolution.

The present model has been applied to observe the influence of the concentration of small bubbles present in the glass melt on growth rate. We have shown that a large density of bubbles changes the bubble growth rate and that the rise time increases when bubble population is large. Moreover, the average composition of the bubble also changes with bubble concentration.

Finally, we have tried to apply our model to describe the gas concentration in a glass melt due to bubbling. The model predicts the transient evolution of redox state which tends to reach an equilibrium between the two phases; however, the equilibrium time is very large compared to experimental reality. The calculations have been also performed taking into account the effect of redox reactions on the diffusion process of O_2 by changing the diffusion coefficient. We have also modified the mass transfer coefficient due to the vigorous convection of bubbling flow. Both of these modifications do not, however, significantly improve the results.

In order to improve the coupled model in the future, it is essential to take convection into account. This insertion of our model into a CFD software might be one way to achieve such a goal.

Nomenclature

Latin symbols

Symbol	Name	Unity
a	bubble radius	m
$C_{\mathfrak{A}_i}$	molar concentration of species \mathfrak{A}_i	mol/m ³
$D_{\mathfrak{G}_j}$	diffusion coefficient of gas \mathfrak{G}_j	m ² /s

G	Gibbs free energy	J/mol
h	glass height	m
H	enthalpy	J/mol
K_r	equilibrium constant of reaction r	–
$L_{\mathfrak{G}_j}$	solubility of gas \mathfrak{G}_j	mol/(m ³ .Pa ^{$\alpha_{\mathfrak{G}_j}$})
\mathbb{M}	matrix in equation (21)	m ³ /mol
M_{rk}	matrix coefficient of \mathbb{M}	m ³ /mol
$n_{\mathfrak{G}_j}$	mole number of gas \mathfrak{G}_j	mol
N_b	concentration number of bubbles	m ⁻³
N_{fg}	number of fining gases	–
N_g	number of gases	–
N_I	number of ionic species	–
$N_{n,fg}$	number of non-fining gases	–
P	total pressure in bubble	Pa
P_0	atmospheric pressure above melt	Pa
$P_{\mathfrak{G}_j}$	partial pressure in bubble of gas species \mathfrak{G}_j	Pa
$Pe_{\mathfrak{G}_j}$	Péclet number of gas \mathfrak{G}_j	–
R	number of reactions	–
\mathcal{R}	universal gas constant	J/(mol.K)
Re	Reynolds number	–
S	entropy	J/(mol.K)
S_{b,\mathfrak{G}_j}	sink term of species \mathfrak{G}_j	mol/(m ³ .s)
$Sh_{\mathfrak{G}_j}$	Sherwood number of gas \mathfrak{G}_j	–
T	temperature	K
u_b	bubble velocity relative to molten glass	m/s
V	bubble volume	m ³
z	vertical position	m

Greek symbols

Symbol	Name	Unity
$\alpha_{\mathfrak{G}_j}$	stoichiometric coefficient on Henry' law of gas species \mathfrak{G}_j	–
β_{rj}	stoichiometric coefficient of reaction r for gas species \mathfrak{G}_j	–
ν_{ri}	stoichiometric coefficient of reaction r for ionic species \mathfrak{A}_i	–
σ	surface tension	N/m
μ	dynamic viscosity	Pa.s
ρ	density	kg/m ³
ζ_r	degree of advancement of reaction r	mol/m ³

References

- [1] R. G. C. Beerkens. Analysis of advanced and fast fining processes for glass melts. In *Advances in Fusion and Processing of Glass III*, pages 3–24. American Ceramic Society, New York, 2003.
- [2] R. G. C. Beerkens and H. de Waal. Mechanism of oxygen diffusion in glassmelts containing variable-valence ions. *J. Am. Ceram. Soc.*, 73:1857–1861, 1990.
- [3] X. Chavanne, J.-M. Flesselles, and F. Pigeonneau. Bubbling laws in a glass furnace. *Verre*, 9(2):6–8, 2003.
- [4] R. Clift, J. R. Grace, and M. E. Weber. *Bubbles, Drops, and Particles*. Academic Press, New York, 1978.

- [5] R. H. Doremus. *Glass Science*. John Wiley & Sons, New York, 1973.
- [6] F. Feuillebois. Some theoretical results for the motion of solid spherical particles in a viscous fluid. *Multiphase Science and technology*, 4:583–789, 1989.
- [7] J. Kloužek and L. Němec. Modelling of glass refining kinetics. Part 2: Bubble distribution models and methods of measurement of refining properties. *Ceramics*, 47:155–161, 2003.
- [8] V. G. Levich. *Physicochemical hydrodynamics*. Prentice Hall, Englewood Cliffs, N.J., 1962.
- [9] J. Matyas and L. Němec. Behaviour of bubble files in glass melting space. *Glastechn. Ber.*, 76:71–80, 2003.
- [10] L. Němec and J. Kloužek. Modelling of glass refining kinetics. Part 1: single bubbles. *Ceramics*, 47:81–87, 2003.
- [11] I. Prigogine and D. Kondepudi. *Thermodynamique. Des moteurs thermiques aux structures dissipatives*. Odile Jacob, Paris, 1999.
- [12] C. Rssel. Redox reactions during cooling of glass melts - A theoretical consideration. *Glass Sci. Technol.*, 62:199–203, 1989.
- [13] H. A. Schaeffer, T. Frey, I. Lh, and F. G. K. Baucke. Oxidation state of equilibrated and non-equilibrated glass melts. *J. Non-Cryst. Solids*, 49:179–188, 1982.
- [14] O. Stahlavsky, J. Brada, M. Trochta, and L. Němec. The bubble effect on the redox state of glass. In *VIII International Seminar on Mathematical Modelling and Advanced Numerical Methods in Furnaces Design and Operation*, Velk Karlovice, 2005.

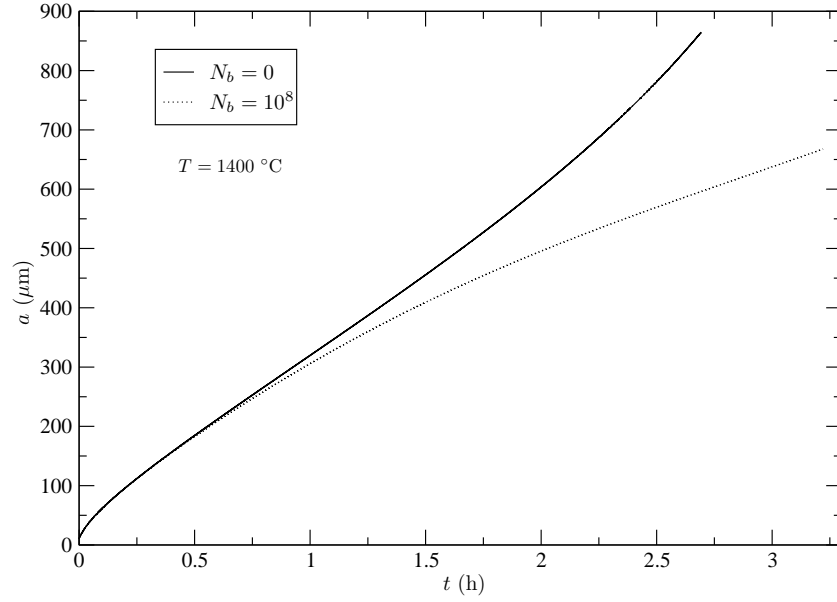


Figure 1: Increase of bubble radius as a function of time with $N_b = 0$ and $N_b = 10^8$ bubbles/m³.

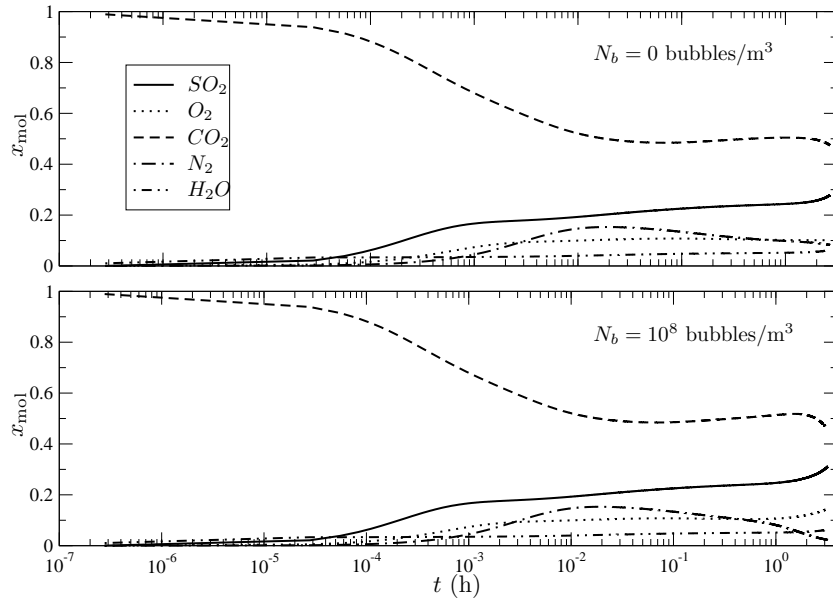


Figure 2: Variation of the molar fraction of gases in bubbles as a function of time with $N_b = 0$ and $N_b = 10^8$ bubbles/m³. x_{mol} is the molar fraction.

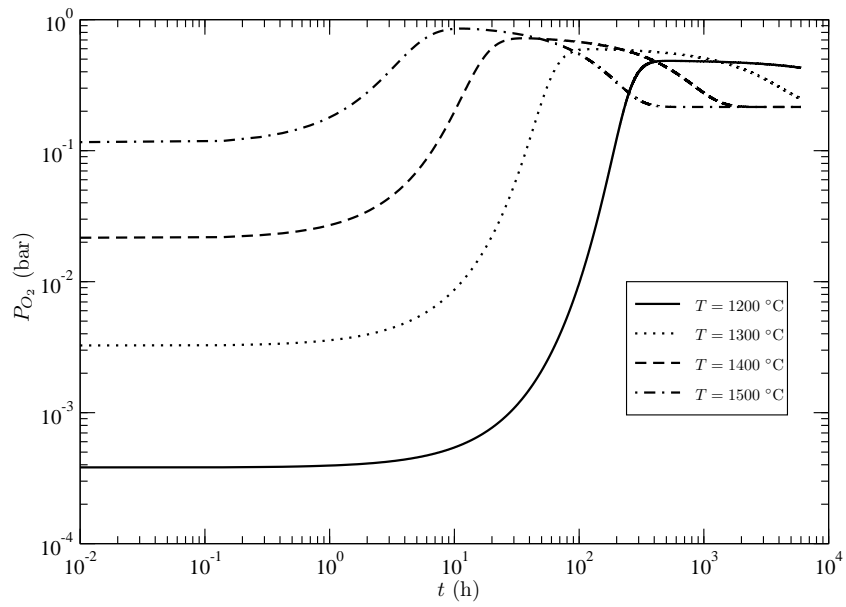


Figure 3: Evolution of O_2 activity of float glass melt as a function of time for $T = 1200, 1300, 1400$ and 1500 °C during bubbling with air.

Reac.	ΔH_r (J.mol ⁻¹)	ΔS_r (J.mol ⁻¹ .K ⁻¹)
Iron	$1.18 \cdot 10^5$	51.96
Sulfate	$3.34 \cdot 10^5$	157.22

Table 3: ΔH_r et ΔS_r of iron and sulfate reactions from [1].

Species	$C_{\mathfrak{A}_i}$ or $C_{\mathfrak{B}_i}$ (mol/m ³)
Fe^{3+}	23.6
Fe^{2+}	5.9
SO_4^{2-}	87.36
SO_2	1.14
O_2	$3.37 \cdot 10^{-4}$

Table 4: Ionic and gas concentrations at $T = 1200$ °C.

Species	$C_{\mathfrak{B}_i}$ (mol/m ³)
CO_2	0.682
N_2	$2.1 \cdot 10^{-2}$
H_2O	38

Table 5: Non-fining gas concentrations in the glass.

Gas	SO_2	O_2	CO_2	N_2	H_2O
Molar fraction	0.28	0.10	0.47	0.08	0.06

Table 6: Molar fraction of gas species in the bubble at the end of evolution with $N_b = 0$.

Gas	SO_2	O_2	CO_2	N_2	H_2O
Molar fraction	0.31	0.15	0.45	0.02	0.06

Table 7: Molar fraction of gas species in the bubble at the end of evolution with $N_b = 10^8$.

T (°C)	1200	1300	1400	1500
a (mm)	30.5	24.3	20.3	18.0
N_b (m ⁻³)	$3.50 \cdot 10^3$	$7.07 \cdot 10^3$	$1.22 \cdot 10^4$	$1.82 \cdot 10^4$

Table 8: Calculated a and N_b at $T = 1200, 1300, 1400$ and 1500 °C for a gas flow rate equal to 2 l/min under standard conditions.